Computers in Biology and Medicine 194 (2025) 110570

Contents lists available at ScienceDirect

Computers in Biology and Medicine

journal homepage: www.elsevier.com/locate/compbiomed

# HADDOCK-Guided modeling and molecular simulations of cereblon-based ternary complexes: Development of novel PROTACs for Ataxia telangiectasia and RAD3-Related (ATR) kinase

Anne-Christin Sarnow [a], Husam Nassar [a], Abdallah M. Alfayomy [a,b], Dina Robaa [a], Wolfgang Sippl [a,*]

[a] Department of Medicinal Chemistry, Institute of Pharmacy, Martin-Luther University Halle-Wittenberg, 06120 Halle (Saale), Germany
[b] Department of Pharmaceutical Chemistry, Faculty of Pharmacy, Al-Azhar University, Assiut, 71524, Egypt

ARTICLE INFO

*Keywords:*
Ataxia telangiectasia and RAD3-Related (ATR) kinase
HADDOCK
Protein-protein docking
Proteolysis targeting chimera (PROTAC)
Cereblon
Ternary complex modeling
Molecular dynamics simulation

ABSTRACT

Proteolysis-targeting chimeras (PROTACs) offer a novel therapeutic strategy for degrading disease-causing proteins, but designing effective degraders remains challenging. PROTACs function by inducing a ternary complex between the target protein and an E3 ligase, requiring structural insights for rational design. Key factors include linker optimization, attachment points, and warhead refinement. Computational approaches, particularly protein-protein docking, are essential for modeling ternary complexes and predicting critical interactions. However, existing docking methods struggle with cereblon (CRBN)-based ternary complexes. To address this, we introduce a computational approach combining HADDOCK protein-protein docking with induced fit PROTAC docking. Validated against 26 crystal structures from the Protein Data Bank (PDB), this method demonstrated high accuracy, especially for CRBN-based complexes. Additionally, molecular dynamics (MD) simulations of CRBN-BRD4-BD1 complexes (PDB IDs 6BN7, 6BOY) provided insights into complex stability through buried surface area and radius of gyration calculations. This validated approach was then applied to five Ataxia telangiectasia and RAD3-related (ATR) kinase PROTACs, enabling modeling in the absence of experimental structures. Our method provides a robust framework for optimizing and designing novel PROTACs targeting diverse proteins.

## 1. Introduction

Proteolysis-targeting chimeras (PROTACs) present a promising and novel approach for therapeutic interventions by inducing the degradation of target proteins via the ubiquitin-proteasome system [1–3]. Structurally, PROTACs are heterobifunctional degraders that consist of two small molecules: one binding to the target protein and the other recruiting an E3-ligase. These two binding moieties are connected by a linker. The simultaneous binding to the target protein and the E3 ligase induces the formation of a ternary complex. In addition, the E3 ligase recruits an E2 ligase, which ubiquitinates lysine residues of the target protein which is subsequently recognized and degraded by the 26S proteasome [4–6]. Despite the variety of target proteins that can be addressed by PROTACs, the number of E3 ligases utilized so far remains limited. The most common ones are: Cereblon (CRBN) [7], von Hippel-Lindau (VHL) [8] and inhibitors of apoptosis proteins (IAPs) [9]. CRBN binders, thalidomide and its analogs pomalidomide and lenalidomide, are frequently used in PROTAC design. This is attributed to their favorable physicochemical properties, such as molecular weight, lipophilicity and bioavailability [10]. Seven CRBN-based PROTACs are currently in clinical trials, all of them being orally administered [11]. This demonstrates the therapeutic potential of PROTACs in targeting various diseases, including cancer, viral infections, and cardiovascular disorders [12–15].

Compared to traditional small molecule inhibitors, PROTACs offer several advantages. By utilizing the cell's natural protein degradation machinery, PROTACs facilitate the selective degradation of disease-causing proteins. This approach can yield a more durable therapeutic effect, as target proteins are permanently eliminated from the system rather than merely inhibited [16]. Additionally, PROTACs require only transient target binding, which enables the targeting of otherwise "undruggable" proteins [17,18]. Furthermore, PROTACs can degrade

* Corresponding author.
*E-mail address:* wolfgang.sippl@pharmazie.uni-halle.de (W. Sippl).

https://doi.org/10.1016/j.compbiomed.2025.110570
Received 5 March 2025; Received in revised form 28 May 2025; Accepted 10 June 2025
Available online 13 June 2025

multiple copies of the target protein, allowing them to act effectively at sub-stoichiometric concentrations [16]. This attribute reduces the risk of off target effects and minimizes toxicity. Notwithstanding their therapeutic potential, the design and application of PROTACs face several challenges. Their properties often exceed Lipinski's "rule of five", potentially leading to limited bioavailability and metabolic instability [19,20]. Moreover, their efficacy is influenced by all three components, with the linker posing particular challenges. The linker must bridge the target protein and E3 ligase with an optimal length and rigidity. Additionally, the attachment points to the warheads further complicate the synthesis of effective PROTACs [21,22].

Computational modeling plays a crucial role in addressing these challenges by providing insights into the binding mechanisms and structural dynamics of PROTACs [23]. Among the established methods, protein-protein docking is a widely used method to generate ternary complex models. This approach has gained prominence due to the availability of experimentally determined crystal structures of ternary complexes, that serve as templates and validation benchmarks [24–27]. A widely recognized protein-protein docking approach was introduced by Drummond et al., with "Method 4B″ within the modeling software MOE [24]. This method involves rigid protein-protein docking using two binary complexes: One consisting of the target protein bound to its warhead and the other compromising the E3 ligase and its corresponding binder. Conformational ensembles of the PROTACs are generated and subsequently combined with the protein-protein docking results. Unfortunately, this method was unable to accurately reproduce CRBN-based ternary complexes, such as PDB IDs 6BN7 and 6BOY [24]. Similarly, alternative strategies like the FRODDOCK-based docking method by Weng et al. have faced limitations with CRBN-based complexes [26]. Consequently, these challenges underscore the need for more accurate modeling approaches to effectively predict CRBN-based complex structures. The modeling of ternary complexes provides a static representation of the protein arrangements and protein interactions, as well as valuable insights into the optimal linker length for PROTACs. Nevertheless, further computational techniques are required to better understand the dynamic behavior of ternary complexes. Previous studies, such as those by Wurz et al. and Harish Kumar et al., have demonstrated the value of molecular dynamics simulations (MDs) in analyzing ternary complexes. They also employed buried surface area (BSA) calculations to assess the strength and stability of the protein-protein interface [28,29]. Despite their utility, the results of the MD simulation must be interpreted cautiously. While experimental evidence suggests that stable complexes are associated with efficient target degradation [30–33], highly rigid PROTACs do not always enhance degradation efficiency [34,35]. Furthermore, the precise stability duration required for ubiquitin transfer and subsequent degradation remains unclear. Moreover, MD simulations are inherently limited in predicting properties such as permeability, bioavailability, or drug efflux, which are critical for assessing the overall efficacy of a PROTAC. Despite these limitations, MD simulations remain powerful tools for providing detailed insights into the conformational flexibility and interaction dynamics of ternary complexes.

In this study, we present a comprehensive approach for modeling ternary complexes, with a particular focus on CRBN-based PROTACs. This approach combines protein-protein docking using High Ambiguity Driven protein-protein Docking (HADDOCK) [36,37] with subsequent induced-fit docking of the PROTAC [38]. HADDOCK employs a semi-flexible docking strategy, distinguishing it from other methods, such as those introduced by Drummond et al. During the refinement step, residues at the protein-protein interface are allowed to move, optimizing the docking pose [36,37]. As HADDOCK does not incorporate the PROTAC during the protein-protein docking, it is docked into the resulting protein-protein conformation using induced-fit docking [38]. In order to validate the approach, we used a dataset of 26 ternary complex crystal structures, involving three E3 ligases (CRBN, VHL and cIAP) and various target proteins. The validation was performed using three key parameters: the Cα root mean square deviation (RMSD) of the protein backbones and the PROTAC RMSD with respect to the crystal structures as well as a comparison of the number of protein-protein interactions. To further investigate the dynamic behavior of CRBN-based ternary complexes, we subjected PDB IDs 6BOY and 6BN7 to 500 ns MD simulations. In addition to RMSD calculations and interaction occupancies between PROTAC and proteins, the BSA and radius of gyration (Rg) were analyzed.

The validated modeling protocol was then applied to model ternary complexes of Ataxia telangiectasia and RAD3-related (ATR) kinase [39], for which we recently developed PROTACs [40]. In addition to our in-house PROTACs, we used other CRBN-based PROTACs with different warhead structures and linker lengths [41,42]. By applying this protocol to ATR-PROTACs, we simulated real-life scenarios where experimental crystal structures may not be available. This not only demonstrates the utility of the protocol but also highlights the potential of computational modeling to guide PROTAC design.

## 2. Materials and methods

### 2.1. Protein preparation

The subsequent preparation steps were performed using the Maestro program in Schrödinger 2021 version 1 [43]. All protein structures were obtained from the Protein Data Bank (PDB; https://www.rcsb.org/). Water and buffer molecules were initially removed from the structures. The Protein Preparation Wizard in Schrödinger was then used to prepare the protein structures [44,45]. Th [46,47]is process included the addition of hydrogens, the assignment of bond orders and the reconstruction of missing side chains and loops. The hydrogen bond network was subsequently optimized by applying PROPKA at pH 7.0. Finally, restrained minimization was performed using the OPLS4 force field with a 0.3 Å RMSD cutoff for heavy atoms [46–49].

### 2.2. Ligand preparation

The PROTAC structures were prepared with the LigPrep tool in Schrödinger 2021 version 1 [50]. Protonation states were generated at pH 7.0 ± 1.0 using Epik [44,51] and energy minimization was performed with the OPLS4 force field. For PROTACs with stereocenters, the stereoisomer was taken from the crystal structure. In the case of ATR CRBN PROTACs, the CRBN ligand was generated analogously in the S-configuration.

Furthermore, ATR inhibitors and CRBN binders were also prepared using LigPrep. Subsequently, the ConfGen tool was employed to generate up to 64 minimized conformers for ATR and CRBN binders [52].

### 2.3. Optimization of the ATR AlphaFold model

The AlphaFold structure for the human ATR kinase was obtained from the AlphaFold website (https://alphafold.ebi.ac.uk/) and the residue range Phe1487 – Met2644 was selected for the subsequent optimization process. The optimization was performed twice, each based on a distinct hinge-binding motif of ATR inhibitors. Two PDB structures of rationally designed PI3K-alpha mutants, which mimic ATR, were used to guide this process: PDB IDs 5UL1 and 5UK8. The ligand in PDB 5UL1 (3-amino-6-(4-{[(2S)-1-(dimethylamino)propan-2-yl]sulfonyl}phenyl)-N-phenylpyrazine-2-carboxamide) features a 2-aminopyrazine hinge-binding motif, whereas the crystalized ligand in PDB 5UK8 ((R)-4-(6-(1-(cyclopropylsulfonyl)cyclopropyl)-2-(1H-indol-4-yl)pyrimidin-4-yl)-3-methylmorpholine) contains a morpholine hinge-binder moiety [53]. In the first step, the ligands were placed in the AlphaFold structure. To this end, a sequence and structural alignment of the catalytic domain (residues 765–1051) from PDB IDs 5UL1 and 5UK8 was performed on the AlphaFold structure using MOE [38]. The ligands from the crystal

structures were then individually placed in the AlphaFold model. Following this, both model structures were prepared using the Protein Preparation Wizard as described above. For the AlphaFold model containing the aminopyrazine ligand, a different rotamer of the Lys2327 residue was manually selected in Maestro.

### 2.4. Molecular docking

Molecular Docking of ATR inhibitors in the PDB structures (PDB IDs 5UL1 and 5UK8) and AlphaFold models was performed using Glide in SP mode [54–58]. The same protocol was implemented for docking CRBN binders in in the CRBN-pomalidomide complex (PDB ID 6H0G). Receptor grid boxes with dimensions of 10 × 10 × 10 Å were generated around the co-crystalized ligands (PDB IDs 5UL1, 5UK8 and 6H0G) or complexed ligands (AlphaFold models) using the Receptor Grid Generation panel. For each ligand, up to 100 poses were generated and subjected to post-docking minimization. Default settings were maintained for all other parameters. Hydrogen bond constraints were applied during docking for ATR inhibitors as follows: Val851-*NH* and Glu849-*CO* (PDB ID 5UL1), Val2380-*NH* and Glu2378-*CO* (AlphaFold model with aminopyrazine inhibitor), Val851-*NH* (PDB ID 5UK8), and Val2380-*NH* (AlphaFold model with morpholine inhibitor). Resulting docking poses were then ranked according to their respective docking scores. The docking protocol was validated by redocking the co-crystalized ligands in PDB IDs 5UL1, 5UK8 and 6H0G, followed by RMSD calculations of the binding pose compared to the crystalized ligands. RMSD values $< 2$ Å were obtained for the three ligands (5UL1: 1.6 Å, 5UK8: 1.3 Å and 6H0G: 0.8 Å).

### 2.5. Ternary complex modeling

In general, the approach can be divided into four main steps. Initially, active residues for the target protein and the E3 ligase must be selected, as these are crucial to guide the protein-protein docking in HADDOCK during the second step. In the third step, the PROTAC is docked in the protein-protein conformation using induced fit docking with pharmacophore placement. Finally, the ternary complexes are simulated for 500 ns, followed by calculations of the RMSD, the buried surface area (BSA) and the radius of gyration (Rg).

#### 2.5.1. Protein-protein docking

Protein-protein docking was performed using the HADDOCK 2.4 web server (https://rascar.science.uu.nl/haddock2.4/) [36,37]. To validate the docking protocol, 26 experimentally determined ternary complex structures were used. In these cases, the PROTAC linker was removed and the protein complexes were split into two substructures: the protein of interest (POI) and the E3 ligase with its corresponding warheads. The details of the POI, E3 ligase, and PROTAC in each structure are provided in Table S1. Additionally, a case study was conducted on two CRBN-based ternary complexes (PDB IDs 6BOY and 8RQ9) to evaluate the impact of using unbound protein structures as input for HADDOCK. Unbound protein structures were selected as follows: CRBN for 6BOY (PDB ID 6H0G), BRD4-BD1 for 6BOY (PDB ID 3MXF), BRD4-BD2 for 8RQ9 (PDB ID 2YEM) and CRBN-midi for 8RQ9 (PDB ID 8RQA) (Table S2).

In order to model ATR kinase ternary complexes, the PROTAC linker was removed, similarly to the validation. The ATR inhibitors docked into the AlphaFold models and the CRBN binders docked into the CRBN structure (PDB ID 6H0G) were utilized for protein-protein docking (Fig. S17 and S18).

Structures for the POI and E3 ligase were prepared separately using the Protein Preparation Wizard, as previously described, and served as input structures for the protein-protein docking. HADDOCK employs a three-stage docking protocol, including rigid-body docking, semi-flexible refinement, and Cartesian-space refinement in explicit solvent [59]. Active residues must be defined for the docking process, as they are restrained to be part of the protein-protein interface. Residues within a radius of 6 Å around the warheads for the POI and E3 ligase were selected in Schrödinger. Their solvent-accessible surface area (SASA) was calculated using the Binding Surface Area Analysis panel. Only residues with a solvent-accessible surface area (SASA) $\geq$ 40 % were specified as active residues, while no passive residues were defined (Fig. S1A and S1B). All other parameters in the HADDOCK 2.4 web server were kept at their default settings. In the docking output, HADDOCK clustered the protein-protein poses based on the fraction of common contacts, a measure of the similarity in intermolecular interactions. The clusters were ranked based on the HADDOCK score, which incorporates various energy components, including intermolecular van der Waals and electrostatic energies, as well as the buried surface area. The HADDOCK score for each cluster was calculated as the average score of its top four members. For the 26 crystalized ternary complexes, all generated protein-protein conformations across all clusters were evaluated. As validation parameter the Cα RMSD of the protein backbones relative to the experimentally determined structures was measured (P-P Cα RMSD). The P-P Cα RMSD was calculated by aligning the entire ternary complex on the Cα atoms of both protein backbones. The conformation with the lowest RMSD, as well as a conformation from the top-scored cluster were selected for further modeling. In the case of ATR PROTACs, a protein-protein conformation from the highest-scoring cluster was chosen for subsequent PROTAC modeling.

#### 2.5.2. Induced fit docking

To complete the modeling of the ternary complexes, PROTACs were docked into the selected protein-protein conformations using molecular docking in MOE [38]. PROTAC structures, including those from crystalized ternary complexes and the ATR kinase, were prepared using LigPrep as previously described. The active sites for the PROTAC docking were defined around the warhead regions in both the POI and the E3 ligase. A combination of pharmacophore placement and the London dG scoring function was employed. The pharmacophore served to guide the placement of the warheads in the respective binding site by identifying critical molecular features necessary for interactions with the POI and E3 ligase (Fig. S1C and S2). Initially, 1000 placement poses were generated in MOE. These poses were then evaluated using the London dG scoring function, which ranks docking poses based on predicted binding affinities. The top 30 ranked poses were further refined using induced fit docking, enabling the receptor side chains to adapt for optimal ligand accommodation. During this refinement, the GBVI/WSA dG scoring function was applied to select the final 5 poses for each docking run. In the end, the top-scored pose of the PROTAC was selected to complete the modeling of the ternary complexes. In order to validate the docking approach, RMSD values were calculated for the heavy atoms of the 26 docked PROTACs relative to the crystalized PROTACs in the ternary complexes (PROTAC RMSD). The final ternary complex models were imported into Schrödinger and prepared using the Protein Preparation Wizard. Protein-protein interactions were analyzed with the Protein Interaction Analysis (Beta) panel and compared with those observed in the crystal structures.

#### 2.5.3. Molecular dynamics simulations

The crystal structures of the BRD4(BD1)-CRBN complexes (PDB IDs 6BOY and 6BN7) and the modeled ATR kinase ternary complexes were subjected to 500 ns MD simulations. For PBD IDs 6BOY and 6BN7 a missing loop (residues 210–218) was added prior to the simulations, using the DDB1-CRBN-pomalidomide complex (PDB ID 6H0G) where this loop is resolved. Furthermore, the stability of the POI and E3 ligase was separately assessed through 100 ns simulations. In this process, the AlphaFold models, the CRBN and BRD structures with their respective warheads were simulated. All system setups and MD simulations were performed using Desmond within the Schrödinger suite [60,61]. Each system was solvated in an orthorhombic box with SPC water molecules, ensuring a distance of 10 Å between the solute structures and the

simulation box boundary. To neutralize the system, Na + or Cl-ions were added, positioned at least 4 Å away from the ligands or PROTACs. The OPLS4 force field and the NPT ensemble were employed for all MD simulations. Each prepared system was initially relaxed using Desmond's relaxation protocol prior to initiating the production simulation. During the production runs, temperature and pressure were maintained at 300 K and 1.01325 bar, respectively, using the Nose–Hoover chain thermostat [62] and the Martyna-Tobias-Klein barostat [63]. The trajectory was recorded at intervals of 100 ps. For the ternary complexes, two independent MD simulation runs were performed with different random seeds. The stability of the AlphaFold model was assessed through three distinct simulations. Simulations of the POI and E3 ligase were conducted once. MD results were analyzed using the Simulation Interaction Diagram (SID) and Simulation Event Analysis (SEA) tools. The SEA module was employed to calculate the P–P Cα RMSD and the RMSD of the ligand over the simulation time, with frame 0 serving as the reference. The P–P Cα RMSD was determined over the simulation time by aligning the entire ternary complex to frame 0 based on the Cα atoms of both protein backbones. This RMSD calculation is consistent with the P-P Cα RMSD measurement used for the validation of the protein-protein docking in HADDOCK (section 2.5.1). The SID tool was used to assess the persistence of ligand-protein interactions over the simulation time. Furthermore, residue-specific flexibility was analyzed by calculating RMSF values using the SID tool. The binding free energy of the ATR ternary complexes was calculated using the Prime MM-GBSA (Molecular Mechanics/Generalized Born Surface Area) panel in Maestro in Schrödinger 2021 version 1. Snapshots were extracted at 1 ns intervals from the final 40 ns of each MD trajectory for the analysis. The structures were solvated using the Variable Solvent Generalized Born (VSGB) solvation model [64] and minimized with the OPLS4 force field, while all other settings were kept at their default values.

#### 2.5.4. Calculation of the BSA and Rg

Based on the MD simulation results, the buried surface area (BSA) and the radius of gyration (Rg) [65] were calculated for the ternary complexes (PDB IDs 6BOY and 6BN7) and the modeled ATR complexes. The Rg was computed using the plot function in the trajectory player of the Schrödinger suite. In this process, all atoms of the ternary complex were selected and the Rg was calculated over the simulation time. Visual Molecular Dynamics (VMD) software [66] was used to calculate the BSA. Initially, the trajectory generated by Desmond was imported into VMD and the first frame was saved in PDB format to serve as the topology file. The trajectory was then saved in DCD format. To compute the BSA, the solvent-accessible surface area (SASA) of the ternary complex components POI, E3 ligase, and PROTAC was calculated separately, as well as for the POI-PROTAC, E3 ligase-PROTAC, and POI-E3 ligase complexes. The BSA of each individual component (POI and E3 ligase) and the protein-protein complex was calculated. The total BSA was determined by summing the individual BSA values for the POI, E3 ligase, and the protein-protein complex as follows:

$$BSA_{POI} = (SASA_{POI} + SASA_{PROTAC}) - SASA_{POI-PROTAC\ complex}$$

$$BSA_{E3\ ligase} = \left(SASA_{E3\ ligase} + SASA_{PROTAC}\right) - SASA_{E3\ ligase-PROTAC\ complex}$$

$$BSA_{prot-prot\ complex} = \left(SASA_{POI} + SASA_{E3\ ligase}\right) - SASA_{POI-E3\ ligase\ complex}$$

$$BSA_{total} = BSA_{POI} + BSA_{E3\ ligase} + BSA_{prot-prot\ complex}$$

## 3. Results and discussion

### 3.1. Validation of the ternary complex modeling

As a first step, the ternary complex modeling approach, combining protein-protein docking in HADDOCK and induced fit ligand docking in MOE, was validated. A set of 26 experimentally derived ternary complex structures deposited in the PDB was used for this purpose. Initially, the PROTAC linker was removed and the structures of the POI and the E3 ligase with their respective warheads were prepared separately for the protein-protein docking in HADDOCK. In a case study on two CRBN-based ternary complexes (PDB ID 6BOY and 8RQ9), unbound crystal structures were utilized for the POI and E3 ligase to assess the impact of employing unbound input structures. Residues within a radius of 6 Å around the ligands and a SASA ≥40 % were selected as active residues in the docking setup. The RMSD of all obtained protein-protein conformations with respect to the native conformations, i.e. corresponding PDB structures, was calculated. The top-scored cluster as well as the model with the lowest P-P Cα RMSD to the native conformation were selected for further evaluation. The number of hydrogen bonds and salt bridges between the POI and E3-ligase were calculated and compared to those observed in the native conformation. Additionally, the respective PROTACs were docked into the selected models and the RMSD of the obtained poses was calculated with respect to the binding mode in the corresponding crystal structures.

The overall method's performance was assessed based on three parameters: the P-P Cα RMSD and PROTAC RMSD of the selected model with respect to the corresponding crystal structure, as well as the number of protein-protein interactions (Table 1, Table 2 and Table S2). Further details concerning the HADDOCK score of the clusters and the docking scores for the PROTAC docking are provided in Table S3.

Drummond and William used a P-P Cα RMSD limit of 10 Å for validating protein-protein docking approaches [24]. Using HADDOCK, the top-scored clusters of 19 out of 26 ternary complexes showed a P-P Cα RMSD <10 Å with respect to the native conformations. Especially for CRBN-complexes, all top-scored clusters showed high resemblance to the native conformation with RMSD values between 0.7 and 3.8 Å, hence confirming that HADDOCK can accurately predict the native protein-protein conformation. Among all protein-protein complexes obtained from HADDOCK, complexes with P-P Cα RMSD values of less than 7 Å were obtained for all tested 26 ternary complexes, with the majority exhibiting RMSDs under 4 Å. Additionally, the complexes showing the highest conformity with the native conformation demonstrated a high degree of similarity between the interactions of the modeled complexes and those observed in the crystal structures. Table S4 presents the hydrogen bonds between the BRD4-BD1 and the CRBN in the ternary complexes of PDB IDs 6BOY, 6BN7, 6BN8 and 6BN9 in comparison to the corresponding models. Besides the number of interactions, also the participating residues of the two proteins were reproduced. Key interactions observed across all complexes include those between Gln78 (BRD4-BD1) and Gln100 (CRBN), as well as between Asp145 (BRD4-BD1) and Hie103 (CRBN). These results obtained for the protein-protein interactions, along with the results for the P-P Cα RMSD further support the right selection of active residues in the protein-protein docking.

To further assess the robustness of the protocol under more practical conditions, unbound protein structures were used as input for two representative CRBN-based ternary complexes (PDB IDs 6BOY and 8RQ9). In both cases, the resulting protein-protein docking solutions closely matched those obtained using the bound crystal structures. For PDB IDs 6BOY and 8RQ9, the protein-protein conformation with the lowest P–P Cα RMSD was still located within the top-scored cluster (RMSD = 1.47 Å and 1.91 Å, respectively, compared to 1.30 Å and 1.24 Å using bound structures) (Table S2). These findings demonstrate the robustness of the HADDOCK protocol, even when applied to unbound input structures. This level of consistency can be attributed to the semi-flexible docking algorithm of HADDOCK, which permits conformational adjustments of protein side chains at the interaction interface.

Notably, complexes with fewer protein-protein interactions tended to demonstrate higher RMSD values during the validation. This tendency highlights the challenge posed by a limited number of interactions during the modeling process, as the modeled complexes often displayed a higher number of predicted protein-protein interactions. These

**Table 1**
Summary of the results obtained for the CRBN-based ternary complex crystal structures used for method validation. The results for the protein-protein conformation with the lowest P-P Cα RMSD as well as the conformation in the top-scored cluster are presented. The results are labeled as follows: * top-scored and[2] 2nd-scored cluster.

| PDB ID | POI | E3 ligase | P-P Cα RMSD [Å] | PROTAC RMSD [Å] | Number of protein-protein interactions | | | |
|---|---|---|---|---|---|---|---|---|
| | | | | | P-P hydrogen bonds | | P-P salt bridges | |
| | | | | | crystal structure | model | crystal structure | model |
| 6BOY | BRD4-BD1 | CRBN | 1.30* | 2.02 | 3 | 3 | 0 | 0 |
| 6BN7 | | | 1.09* | 1.61 | 3 | 4 | 0 | 0 |
| 6BN8 | | | 0.77* | no crystl. ligand | 2 | 2 | 0 | 0 |
| 6BN9 | | | 0.66* | no crystl. ligand | 2 | 3 | 0 | 0 |
| 8RQ9 | BRD4-BD2 | CRBN | 1.24* | 1.47 | 1 | 2 | 0 | 0 |
| 8UH6 | PTPN2 | CRBN | 3.81* | 1,88 | 1 | 2 | 0 | 0 |
| | | | 3.02[2] | 1.06 | | 2 | | 0 |

**Table 2**
Summary of the results obtained for VHL and cIAP based ternary complex crystal structures used for method validation. The results for the protein-protein conformation with the lowest P-P Cα RMSD as well as the conformation in the top-scored cluster are presented. The results are labeled as follows: * top-scored,[2] 2nd-scored,[3] 3rd-scored,[4] 4th-scored,[5] 5th-scored or[6] 6th-scored cluster.

| PDB ID | POI | E3 ligase | P-P Cα RMSD [Å] | PROTAC RMSD [Å] | Number of protein-protein interactions | | | |
|---|---|---|---|---|---|---|---|---|
| | | | | | P-P hydrogen bonds | | P-P salt bridges | |
| | | | | | crystal structure | model | crystal structure | model |
| 7KHH | BRD4-BD1 | VHL | 7.45* | no pose | 2 | 1 | 1 | 0 |
| | | | 1.37[4] | 1.72 | | 2 | | 1 |
| 8BEB | | | 1.91* | 1.89 | 1 | 2 | 0 | 0 |
| 8BDS | | | 0.90* | 1.73 | 2 | 3 | 1 | 1 |
| 5T35 | BRD4-BD2 | VHL | 2.16* | 2.00 | 6 | 7 | 0 | 0 |
| 8BDT | | | 1.99* | 1.79 | 7 | 6 | 3 | 3 |
| 8BDX | | | 17.4* | no pose | 4 | 1 | 1 | 0 |
| | | | 1.44[3] | 1.31 | | 3 | | 1 |
| 6SIS | | | 3.46* | 3.24 | 6 | 4 | 2 | 1 |
| | | | 1.24[3] | 1.02 | | 4 | | 2 |
| 7PI4 | FAK | VHL | 17.5* | no pose | 4 | 5 | 0 | 3 |
| | | | 1.47[4] | 1.37 | | 4 | | 0 |
| 6HR2 | SMARCA4 | VHL | 7.02* | no pose | 4 | 3 | 0 | 1 |
| | | | 2.92[2] | 1.89 | | 4 | | 0 |
| 6HAX | SMARCA2 | VHL | 8.43* | no pose | 3 | 1 | 0 | 0 |
| | | | 3.73[4] | 2.01 | | 3 | | 0 |
| 6HAY | | | 2.26* | 1.52 | 3 | 3 | 0 | 0 |
| 7Z6L | | | 13.6* | no pose | 1 | 5 | 0 | 1 |
| | | | 2.69[6] | 1.53 | | 1 | | 0 |
| 7Q2J | WDR5 | VHL | 10.6* | no pose | 3 | 4 | 1 | 1 |
| | | | 4.00[3] | 2.16 | | 3 | | 1 |
| 7JTP | | | 1.35* | 1.49 | 3 | 5 | 1 | 1 |
| 8BB2 | | | 8.17* | no pose | 1 | 3 | 0 | 0 |
| | | | 6.85[4] | no pose | | 2 | | 0 |
| 8BB3 | | | 12.8* | no pose | 0 | 3 | 0 | 0 |
| | | | 6.14[2] | no pose | | 1 | | 0 |
| 8BB4 | | | 14.8* | no pose | 1 | 2 | 1 | 1 |
| | | | 3.28[5] | 2.28 | | 1 | | 1 |
| 8BB5 | | | 10.2* | no pose | 0 | 1 | 0 | 0 |
| | | | 5.15[3] | no pose | | 2 | | 0 |
| 6W7O | BTK | cIAP | 2.91* | 1.38 | 5 | 4 | 0 | 0 |
| 8DSO | | | 5.9* | no pose | 2 | 2 | 0 | 0 |
| | | | 1.06[4] | 1.55 | | 3 | | 0 |

observations become particularly evident in the WDR5-VHL ternary complex structures (PDB IDs: 8BB2, 8BB3 and 8BB5). In Fig. S3, the missing protein-protein interactions for PDB ID 8BB3 compared to other ternary complexes are visible. The observed discrepancy may, in part, be attributed to the docking algorithm's reliance on predefined active residues. These residues enforce interactions at the interface even when they are absent in the crystal structure. Such constraints can lead to artificially increased protein-protein interactions during docking and reduced accuracy for complexes with inherently sparse interfaces.

As a last step, the PROTACs were docked into the top-scored protein-protein conformation as well as that showing the lowest P-P Cα RMSD to the native conformation. To this end, induced fit docking utilizing pharmacophore features (Fig. S1C and S2) as constraints was conducted in MOE. Induced fit docking effectively addresses the structural complexity of PROTACs by introducing flexibility not only to the ligand but also to the protein binding site. Additionally, the selected pharmacophore features guide the docking procedure by ensuring the correct position of the warheads within the binding site. The RMSDs of the top-scored docking poses were calculated using the respective native conformation of the PROTAC in the corresponding PDB as a reference. Top-scored docking poses displayed RMSD values $< 2.5$ Å compared to their respective crystal structures in all cases where the used protein-protein conformation shows high conformity with the native conformation (P-P Cα RMSD $<5$ Å). Meanwhile, no docking results were obtained in the protein-protein conformations that display P-P Cα RMSDs $>5$ Å. This might be caused by deviations from the native protein-

protein conformation in the modeled ternary complexes preventing the PROTAC from adequately bridging the distance between the two proteins. It's noteworthy that the obtained docking poses in all top-scored protein-protein conformations of CRBN-based complexes showed an RMSD <2.02 Å.

In conclusion, the combination of protein-protein docking in HADDOCK with induced fit ligand docking in MOE represents an accurate approach for modeling ternary complexes of various target proteins and E3 ligases. In Fig. 1, the obtained CRBN-based modeled complexes (PDB IDs: 6BN7, 6BOY and 8RQ9) are illustrated in comparison to their crystal structures. The BRD4-warheads formed hydrogen bonds with an asparagine residue. Similarly, for CRBN warheads, three hydrogen bonds were observed to be formed by the glutarimide moiety with His378 and Trp380 in all displayed PROTACs. Further ternary complexes data are provided in Fig. S3.

While the validation setup in this study provides a more favorable scenario compared to using unbound structures, it ensures consistency across the tested dataset. Importantly, HADDOCK's semi-flexible refinement enables conformational adjustments at the protein-protein interface. This reduces potential bias introduced by starting with

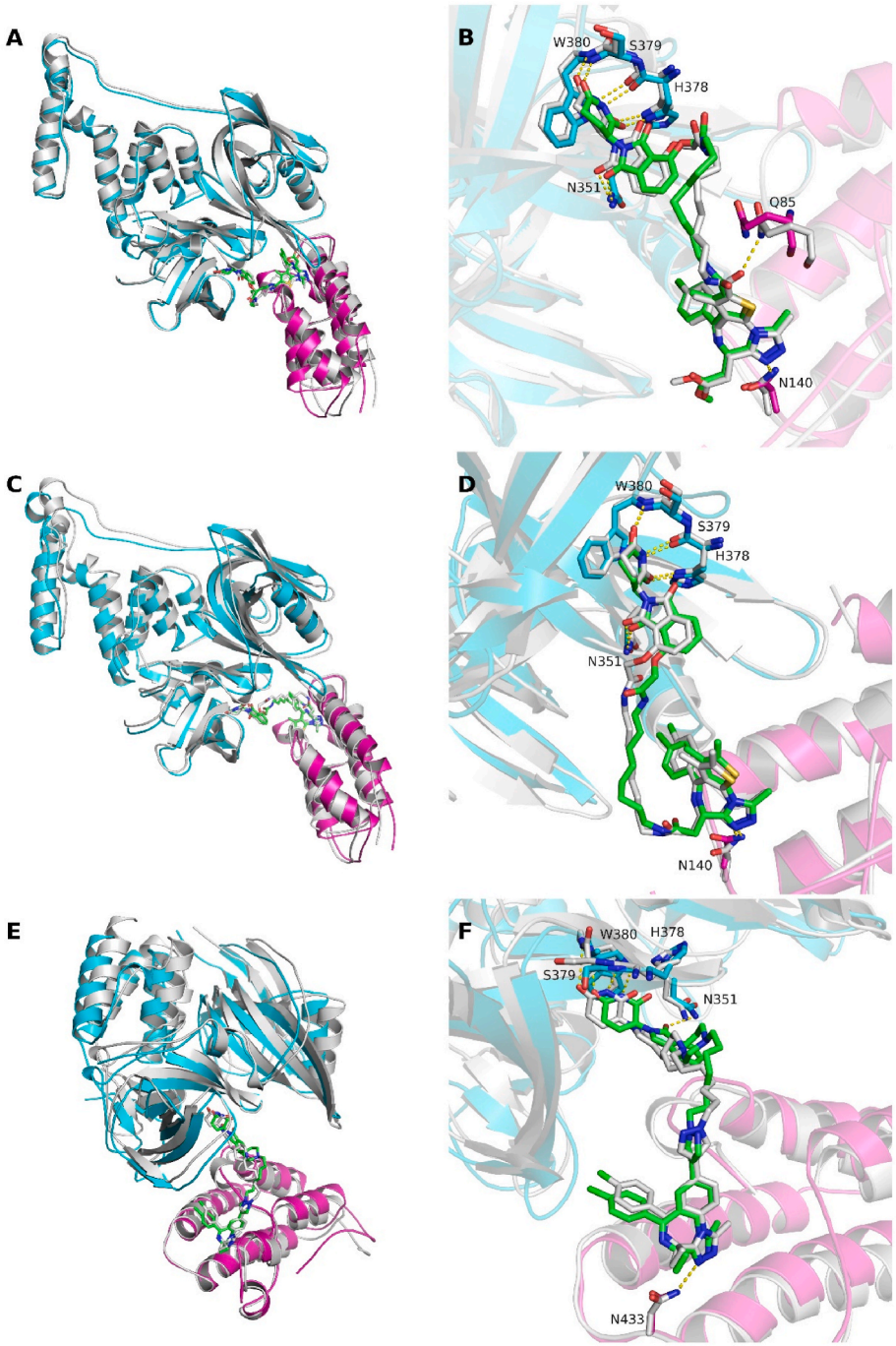


**Fig. 1.** Modeled ternary complexes are shown in comparison to the crystal structures after superposition on the Cα atoms of the protein backbone. Proteins and ligands of the crystal structure are colored white. For the modeled complexes, the protein of interest is shown in cyan, CRBN in magenta and the ligand as green sticks. Important binding site residues are shown as sticks and hydrogen bonds are indicated by yellow dashed lines. (A) and (B) BRD4-BD1/CRBN (PDB ID 6BN7). (C) and (D) BRD4-BD1/CRBN (PDB ID 6BOY). (E) and (F) BRD4-BD2/CRBN (PDB ID 8RQ9). (For interpretation of the references to color in this figure legend, the reader is referred to the Web version of this article.)

bound structures, which was further confirmed by using unbound input structures for PDB IDs 6BOY and 8RQ9. In contrast, many benchmarked methods, like Method 4B, are based on rigid-body docking, where the lack of flexibility can make unbound scenarios significantly more challenging. Although these methods were evaluated using unbound proteins, a comparison to the implemented HADDOCK-based approach remains informative even under slightly different modeling conditions. This approach proved to be highly reliable especially in modeling CRBN-based ternary complexes, outperforming previously published methods. For instance, Method 4, implemented by Drummond et al., failed to generate ternary complexes with an RMSD <10 Å for PDB ID 6BOY [25]. Similarly, Method 4b generated only 0.4 % (BRD4-BD1/CRBN, PDB ID 6BOY) and 5.1 % (BRD4-BD1/CRBN, PDB ID 6BN7) of ensembles with RMSD values below this threshold [24]. Meanwhile, the FRODDOCK-based protocol was only capable of producing models of an acceptable quality for CRBN-based ternary complexes within an interface RMSD range of 2.93–4.96 Å [26]. Likewise, Rovers and Schapira's benchmark study revealed the inaccuracy of AlphaFold-Multimer in predicting these protein-protein conformations. For CRBN-based ternary complexes, the predict models exhibited RMSD values > 17 Å, further highlighting the limitations in modeling CRBN-based ternary complexes [67]. In contrast, our HADDOCK-based approach consistently achieved RMSD values ≤ 4 Å for all CRBN-based ternary complexes, with the PROTAC itself exhibiting RMSD values ≤ 2 Å. Additionally, the structure with the lowest RMSD was consistently located within the top-scored cluster. This facilitates the reliable selection of the most accurate protein-protein conformation for CRBN-based PROTACs with unknown protein-protein conformations. To further evaluate the performance of the implemented HADDOCK-based protocol, the comparison of the results was extended to a broader set of VHL-based ternary complexes. In general, Method 4B as well as the FRODOCK-based protocol, achieved higher accuracy for VHL-based ternary complexes than for CRBN-based ones. For instance, in the case of the BRD4-BD2/VHL ternary complexes (PDB IDs 5T35 and 6SIS), FRODOCK produced models with interface RMSD values below 1 Å [26]. Method 4B also performed well, generating 57.9 % of the ensemble for PDB ID 5T35 within the RMSD threshold of 10 Å [24]. In comparison, the implemented HADDOCK-based approach achieved RMSD values of 2.16 Å (PDB ID 5T35) and 3.46 Å (PDB ID 6SIS) for models within the top-scored clusters. Further evaluation was performed on the SMARCA/VHL ternary complexes (PDB IDs 6HAX, 6HAY, and 6HR2). For these complexes, Method 4B and FRODOCK both achieved RMSD values in the range that is typically considered to be crystal-like. Method 4B produced models with RMSD values ranging from 4 to 8.5 Å, while FRODDOCK achieved interface RMSDs below 2 Å [24,67]. Protein-protein docking in HADDOCK generated comparable results with RMSD values between 2.26 and 8.43 Å among the top-scored clusters. As with the CRBN-based systems, AlphaFold-Multimer consistently failed to generate accurate models for VHL-based ternary complexes. All resulting structures displaying RMSD values exceeding 10 Å [67]. These outcomes were notably less accurate than those produced by any of the evaluated protein-protein docking methods, including the implemented HADDOCK-based protocol. As mentioned above, the HADDOCK based approach displayed certain limitations when applied to ternary complexes with fewer protein-protein interactions, like PDB IDs 8BB2, 8BB3, 8BB4 and 8BB5. Similarly, Method 4B failed to generate crystal-like structures in these cases. Our HADDOCK-based approach showed comparably bad results, where only the model of PDB ID 8BB2 displayed an RMSD <10 Å. However, crystal-like poses could still be identified in lower-ranked clusters. This suggests that, despite ranking limitations, HADDOCK retains the potential to generate accurate models in challenging scenarios. Compared to the modeling of CRBN-based ternary complexes in HADDOCK, the model with the lowest RMSD for VHL-based systems was not consistently found within the top-scored cluster. However, the overall performance of the HADDOCK-based protocol remained competitive with other ternary complex modeling workflows. The obtained RMSD values for VHL-based models in the top-scored clusters were within the same range as in previously published methods. These findings indicate that the protocol is also applicable to model VHL-based ternary complexes; however all obtained clusters including the lower-ranked ones have to be taken into consideration particularly in ternary complexes with fewer protein-protein interactions. Nevertheless, ternary complex modeling approaches, such as HADDOCK, have inherent limitations. They cannot predict factors such as PROTAC permeability or bioavailability, which are key elements in achieving effective degradation. However, they do provide valuable insight into protein-protein conformations, linker length, and PROTAC-protein interactions.

### 3.2. MD simulations of ternary complex crystal structures

#### 3.2.1. MD simulations

To assess the stability of CRBN-based ternary complexes and to validate the simulation protocol, MD simulations were performed on the crystal structures (BRD4-BD1/CRBN, PDB ID 6BN7 and 6BOY). Each structure was simulated twice for 500 ns. Prior to simulating the complete ternary complex, the individual warhead-protein complexes (BRD4-BD1 and CRBN) were analyzed using 100 ns MD simulations.

The BRD4-BD1-ligand complex demonstrated high stability, with fluctuations between 1 and 2 Å for the Cα atoms of the protein backbone and ligand RMSDs around 1 Å (Fig. S4). In contrast, the CRBN-thalidomide complex revealed a highly flexible loop region [44,45] as evidenced by the protein RMSF values, which ranged from 3 to 6 Å (Fig. S4C and S5A). This loop typically interacts with the DNA damage-binding protein 1 (DDB1) [68]. As this flexibility does not affect the ligand binding site or the protein-protein interface in the ternary complex, the loop was excluded from further RMSD calculations. The recalculated RMSD for the Cα backbone stabilized at approximately 2 Å (Fig. S4D). The CRBN binder also remained stable with RMSD values < 1 Å, forming stable hydrogen bonds with the backbone of Trp380 and His378. A third hydrogen bond to the side chain of His378 showed a significantly lower occupancy due to side chain flexibility (Fig. S5B).

The crystal structures of BRD4-BD1/CRBN (PDB IDs 6BN7 and 6BOY) exhibit an identical protein-protein conformation, despite incorporating different PROTACs. MD simulations over 500 ns revealed only minor differences in their dynamic behavior. For PDB ID 6BN7, the RMSD of the Cα atoms stabilized between 3 and 4 Å, while for PDB ID 6BOY the protein RMSD initially increased to 5 Å before stabilizing in the same range (Fig. S6). The RMSD of the PROTAC in both complexes remained stable, fluctuating minimally between 1 and 2 Å (Fig. S6, S7 and S9). Furthermore, the interactions between the PROTAC and their respective proteins aligned with the findings from the simulations of the individual warhead-protein complexes. Of particular note were the interactions with the backbones of Trp380 and His378 of CRBN, which displayed the highest stability (Table S5). These results were consistent across the second simulation replicate, which showed similar RMSD trends and hydrogen bond occupancies (Fig. S7–S9).

#### 3.2.2. Calculation of the buried surface area (BSA) and radius of gyration (Rg)

The further validate the stability of the ternary complexes, the radius of gyration (Rg) and the buried surface area (BSA) were analyzed. While the Rg provides a measure of the compactness and resulting structural stability of the ternary complex [11], the BSA offers insights into the stability of the protein-protein interface [69]. Both parameters remained stable throughout the 500 ns simulations, with Rg values between 28 and 29 Å and consistent BSA profiles for both PDB IDs 6BN7 and 6BOY. The results for both replicates are displayed in (Fig. S6 and S7). This consistency suggests that the ternary complexes remained intact throughout the simulation, with no evidence of protein dissociation. Altogether, stable RMSD values for the proteins and ligands, Rg and BSA values validate the MD protocol and confirm the structural robustness of

the complexes. Notably, this stability of PDB ID 6BOY is consistent with findings from Rovers and Schapira, which were obtained using different simulation settings [67].

Nevertheless, the results from MD simulations should be interpreted with caution. Studies, such as those by Kumar et al. or Rovers and Schapira, have demonstrated that even active PROTACs can form ternary complexes that appear unstable in MD simulations [28,67]. This again is particularly evident in cases of ternary complexes with a limited number of protein-protein interactions, as observed in WDR5-VHL-PROTAC ternary complexes (PDB IDs 7Z6L, 8BB2 or 8BB5). These complexes exhibited significant flexibility over the duration of the simulation. Furthermore, longer or more flexible linkers are possibly associated with higher RMSD values, underscoring that instability in MD simulations does not necessarily indicate an inactive PROTAC. Moreover, MD simulations do not account for factors such as permeability or drug efflux of the PROTACs, which can significantly influence the degradation efficacy. Despite these challenges, MD simulations remain an invaluable tool for studying the dynamic behavior of ternary complexes. They provide critical insights into the stability of warhead structures within their respective binding sites, ensuring that the proteins are brought into sufficient proximity for degradation. Moreover, MD simulations facilitate the exploration of linker length and flexibility, offering guidance for the rational design of PROTACs. Importantly, while instability in MD simulations may not rule out the PROTAC activity, observing stability can support the hypothesis that effective degradation is possible. This has been demonstrated previously for BRD4-BD1/VHL complexes (PDB IDs 7KHH and 8BDS), as well as in this study for BRD4-BD1/CRBN-based complexes such as 6BOY and 6BN7 [28].

### 3.3. Modeling of ATR ternary complexes

#### 3.3.1. Optimization of the ATR AlphaFold model

The only available human ATR kinase structure in the PDB (PDB ID 5YZ0) has several missing loops that could not be accurately modeled using classical homology modeling [70]. These missing loops rendered the structure unsuitable for dynamic analysis of ternary complexes. Docking in the initial AlphaFold structure failed because of the unfavorable orientation of several side chains in the binding pocket. Therefore, the structure was subsequently optimized to ensure its suitability for molecular docking and simulation studies. To this end, the binding conformation of two ATR inhibitors, a morpholine- and an aminopyrazine-based ligand, was retrieved from the respective PDB structure (respectively from PDB IDs 5UK8 and 5UL1, obtained from a rationally designed PI3K-alpha mutant that mimics ATR [53]) and inserted in the AlphaFold model. The resulting complexes were subsequently energy minimized, which led to conformational changes in several side chains in the binding pocket. Notably, the orientation of Asp2494 was altered for both ligands, while the aminopyrazine ligand also induced conformational changes in the side chain of Glu2479. To prevent unfavorable clashes between the protein and ligand, an alternative conformer for Lys2327 was selected (Fig. S10A and Fig. S11A). The optimized AlphaFold models underscore the necessity of employing ligand-specific models, as the distinct hinge-binding motifs (morpholine and aminopyrazine) induce differing side chain conformations. The ATR PROTACs used in subsequent modeling phases incorporate both hinge-binding motifs.

Consequently, the minimized AlphaFold models were validated through molecular docking. The docking protocol was previously validated with crystal structures (PDB IDs 5UK8 and 5UL1), yielding RMSD values under 2 Å and confirming the reproducibility of key interactions (Fig. S12). In the AlphaFold models, the binding mode of the ligands was successfully reproduced in both structures. For the aminopyrazine ligand, an RMSD of 1.5 Å was calculated when compared to its position in PDB ID 5UL1. The docking results confirmed the formation of key hydrogen bonds, including two interactions with the hinge region (Val2380 and Glu2378) and a third bond with Gly2385 via the sulfone moiety (Fig. S10B). For the morpholine ligand, an RMSD of 1.2 Å was achieved relative to its position in PDB ID 5UK8. This docking pose included a hydrogen bond between the hinge region (Val2380) and the oxygen of the morpholine ring system, as well as a second bond between Asp2335 and the nitrogen of the indole system (Fig. S11B). The final validation step involved MD simulations to assess the stability of the models. Results obtained for the aminopyrazine-containing model are presented in Fig. S13, while the results for the morpholine model are provided in the SI (Fig. S14). The RMSD values for the entire protein (residues 1487–2644) fluctuated between 3 and 4 Å, while the catalytic domain (residues 2296–2604) stabilized between 2 and 3 Å. For the ligand, stable RMSD values between 1 and 2 Å were achieved. The higher RMSD values for the full protein can be attributed to a flexible loop (residues 1604–1620), which displayed RMSF values between 4 and 8 Å. This loop is absent in the corresponding PDB structure (PDB ID 5YZ0) and has low confidence values in the AlphaFold model (pLDDT $<$50), which likely explains its high flexibility. As this loop does not influence the binding pocket, it is not expected to affect ligand binding. Additionally, there is no indication that it plays a role in the protein-protein interface. Besides the RMSD values below 2 Å, the stability of the ligands was further supported by the hydrogen bond occupancy: the aminopyrazine- and the morpholine moiety exhibited occupancy levels of over 90 % with the kinase hinge region (Val2380 and Glu2378). Additionally, the hydrogen bonds to other residues, like Gly2385 or Asp2335, are maintained for the majority of the simulation (Fig. S15 and S16). In conclusion, the successful docking results and the stable MD simulations confirm that the models are well-suited for ternary complex modeling.

#### 3.3.2. Modeling of ATR/CRBN ternary complexes

The validated methods for the modeling of ternary complexes and the optimized AlphaFold models were finally employed to model ternary complexes for the ATR kinase with CRBN. For this purpose, five recently reported ATR-targeting PROTACs with confirmed degradation activity were selected. Table S6 and Fig. 2 summarize information about the PROTAC structures and degradation effects used during the modeling process. In cellular assays, these PROTACs demonstrated strong ATR degradation. 42i (Abd110) achieved 80–90 % ATR degradation at 1 μM in MV-4-11 cells [71]. Similarly, 8i, 10b, and 12b exhibited high degradation efficiencies in the same cell line at 0.5 μM [41]. Among them, 8i was the most effective PROTAC, achieving 93 % ATR degradation, followed by 10b (86 %) and 12b (81 %). The degradation of 8i, 10b and 12b was evaluated using western blotting. PROTAC ZS-7 induced ATR degradation in ATM deficient LoVo cells. A maximum degradation of 84 % was achieved after 72 h of treatment with a $DC_{50}$ of 0.53 μM [42].

All mentioned PROTACs recruit CRBN as E3 ligase, but the ATR warheads and the linker length differ. In Fig. S17 and S18, the docked warheads into the respective ATR or CRBN structure are illustrated. PROTAC ZS-7 [42] incorporates the morpholine hinger-binding moiety, whilst the remaining four PROTACs feature an aminopyrazine hinge binder. Furthermore, structural variations are observed in the linker region. PROTAC 42i (Abd110) [40] contains a sulfonamide group, whereas PROTACs 8i, 10b and 12b [41] include an amide group. The figures also highlight the active residues selected for the protein-protein docking using HADDOCK. These active residues varied among the PROTACs due to differences in their ATR warhead structures. To account for these structural variations, three separate HADDOCK runs were performed: 42i (Abd110) (run I); 8i, 10b and 12b (run II); ZS-7 (run III). The grouping strategy employed in this study ensured that the distinct structural characteristics of the PROTACs were appropriately addressed during the ternary complex modeling.

In accordance with the HADDOCK validation results, a protein-protein conformation from the top-scored cluster was selected for each docking run. The pharmacophore features utilized to guide the docking

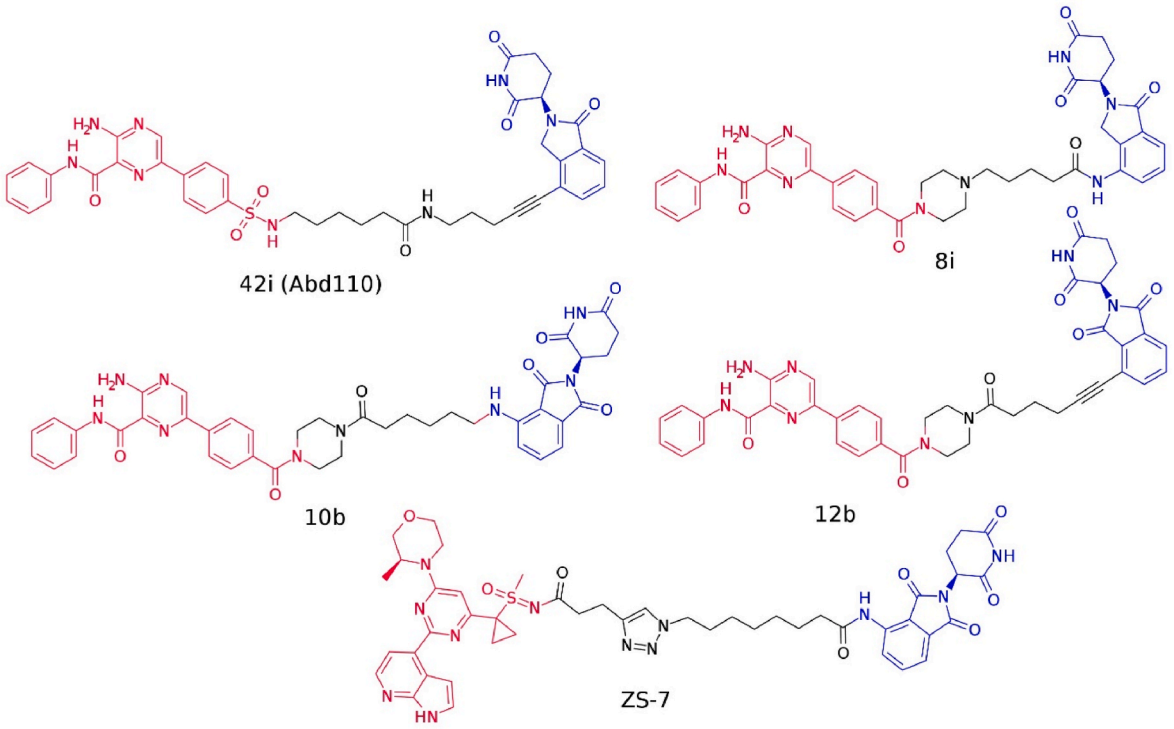


**Fig. 2.** Structures of active ATR PROTACs that are used for the modeling of the ternary complexes. The ATR kinase warheads are colored red, the CRBN warheads are shown in blue and the linkers are highlighted in black. (For interpretation of the references to color in this figure legend, the reader is referred to the Web version of this article.)

of the PROTACs within the selected conformation are presented in Fig. S19. Ternary complexes were successfully generated for all PROTACs, showing the required interactions between PROTACs and their respective protein partners (Fig. 3 and S20). The aminopyrazine moiety (in 42i (Abd110), 8i, 10b and 12b) formed two hydrogen bonds to the ATR kinase hinge region (Val2380 and Glu2378), while the morpholine hinge-binder in ZS-7 interacted only with Val2380. Additional hydrogen bonds were observed between the sulfonamide- or amide groups of the ATR warheads and Gly2385. Furthermore, PROTAC ZS-7 displayed two additional bonds to Lys2327 and Asp2335 in the affinity pocket. All five PROTACs consistently interacted with CRBN through three hydrogen bonds between the glutarimide moiety and Trp380 and His378. A comprehensive summary of the HADDOCK scores and docking scores for the ATR PROTACs is provided in Table S6.

Subsequent alignment of the ternary complexes revealed similar protein-protein conformations across all PROTACs. Despite the variations in warhead structures and active residues used in HADDOCK, the RMSD matrix confirmed this similarity, suggesting that active ATR kinase PROTACs fit the same protein-protein conformation (Table S7 and Fig. 4). This observation aligns with previous findings from the PROTACs in the crystal structures of BRD4-BD1/CRBN (PDB IDs 6BOY and 6BN7). Moreover, for VHL-based ternary complexes of the BRD4-BD1 (PDB IDs 7KHH, 8BEB, 8BDS) and BRD4-BD2 (PDB IDs 5T35, 6SIS, 8BDT, 8BDX), the crystal structures demonstrated similar protein-protein conformations despite different active PROTACs with varying linker lengths.

### 3.3.3. MD simulations of the ATR/CRBN ternary complexes

*3.3.3.1. MD simulations.* In order to evaluate the dynamic stability of the modeled ATR ternary complexes and confirm the validity of the docking results, two independent MD simulations (500 ns) were conducted for each complex. The results revealed stable protein-protein conformations across all PROTACs with protein Cα RMSD values stabilizing at 4 Å after initial fluctuations (Fig. 5 and S21). Minor deviations in the RMSD plots are attributed to flexible loops in the ATR kinase, particularly residues 1604–1620 and 1870–1880, which exhibited higher RMSF values (Fig. S22). The loops are distant from the binding pocket of the PROTAC and are, hence, not expected to affect the stability of the complex at the protein-protein interface. Despite the variation in linker length, all five PROTACs demonstrated consistently stable RMSD values around 2 Å throughout the simulation. This stability is further underscored by the RMSF values, with most atoms displaying fluctuations under 2 Å (Fig. S23). The RMSF plots of the PROTACs indicated that they remained stable during the course of the MD-simulation. Slightly higher flexibility was observed in the linker region of ZS-7, the PROTAC with the longest linker. For the aminopyrazine-based PROTACs, the terminal phenyl group connected via a carboxamide to the aminopyrazine moiety was identified as the most flexible moiety. The stability of the complexes was further supported by consistent ligand-protein interactions. Hydrogen bond occupancies between the aminopyrazine or morpholine moiety and the kinase hinge region (Val2380 and Glu2378) ranged from 70 % to 97 %. Likewise, interactions between the glutarimide moiety of the PROTACs and CRBN Trp380 exceeded 90 %, highlighting consistent binding (Fig. S24–S28). The hydrogen bond, particularly with the side chain of His378, exhibited significantly lower occupancy, which can be attributed to the increased flexibility of this side chain.

Subsequently, MM-GBSA binding free energy calculations for the different ATR PROTACs were performed using snapshots taken every 1 ns from the final 40 ns of each 500 ns MD simulation. These binding free energy calculations provide an estimate of the binding affinity of a protein-ligand complex [72]. Additionally, they have been shown to effectively predict the binding stability of PROTAC-induced ternary complexes [73].

Despite differences in experimental conditions and concentrations, all five PROTACs demonstrated potent degradation activity (80–93 %). Consistently, MM-GBSA calculations yielded negative binding free

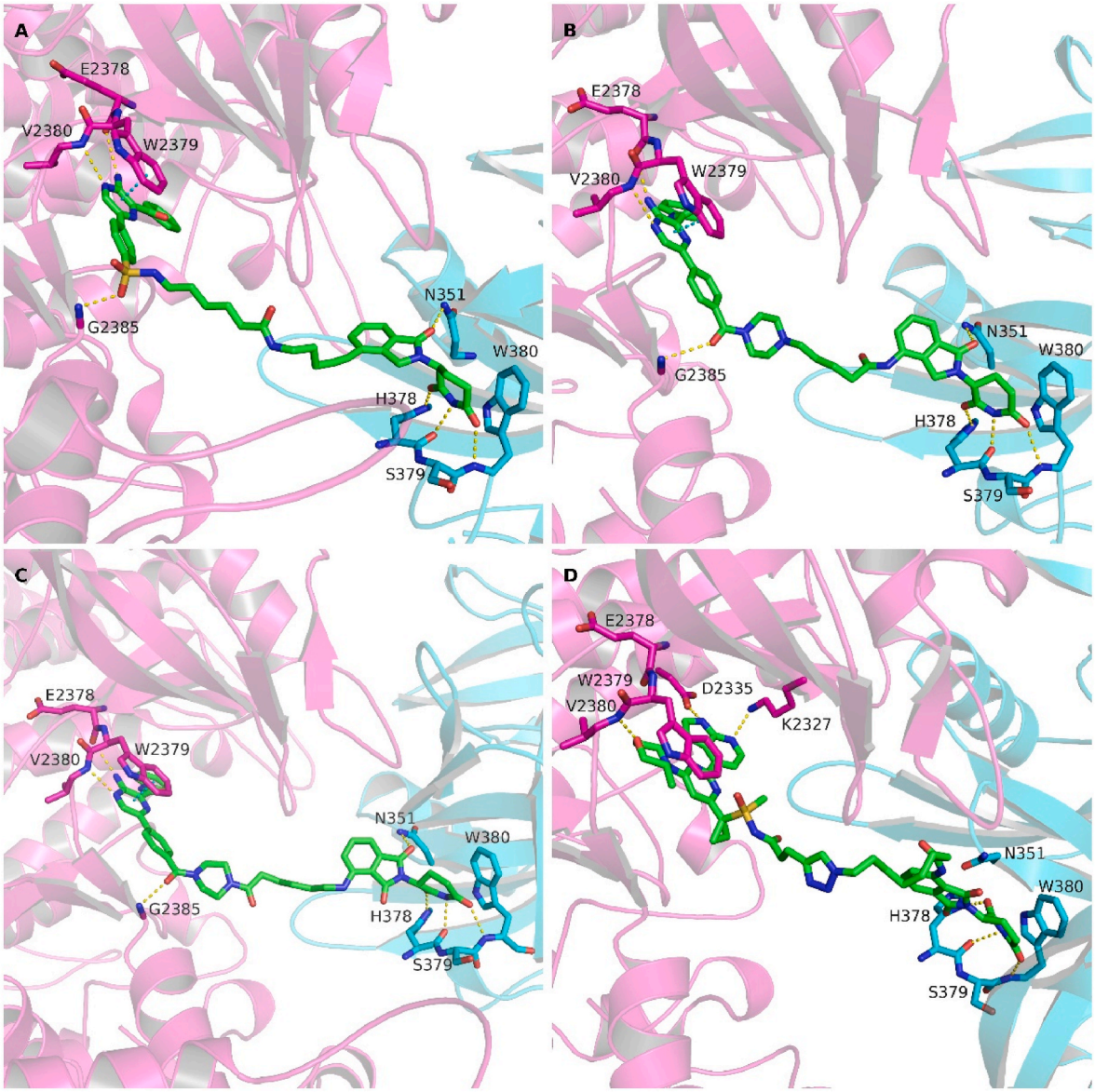


**Fig. 3.** Modeled ternary complexes for the ATR kinase. The protein backbone of ATR is displayed in magenta, while the backbone of CRBN is displayed in cyan. Important binding site residues shown as sticks. The PROTACs are presented as green sticks. Hydrogen bonds are displayed as yellow dashed lines, while pi-pi interactions are indicated by cyan dashed lines. The ternary complexes are shown as follows: (A) 42i (Abd110), (B) 8i, (C) 10b and (D) ZS-7. (For interpretation of the references to color in this figure legend, the reader is referred to the Web version of this article.)

energies below −100 kcal/mol, aligning with their observed degrader activity and supporting their binding stability in the ternary complexes (Table S8). Among the three PROTACs tested under identical experimental conditions (8i, 10b, and 12b), 8i exhibited the most negative binding free energy (below −130 kcal/mol). This aligns with its highest observed degradation efficiency compared to 10b and 12b. It was also found that 42i (Abd110) and ZS-7 displayed highly negative MMGBSA values, indicating favorable ternary complex formation. However, a direct quantitative comparison is limited due to differences in experimental conditions. Standard deviations ranged from 5 to 7 kcal/mol, reflecting fluctuations inherent to MD-based MM-GBSA calculations, but overall trends remained consistent. The use of discrete snapshots may also contribute to this variability. While MM-GBSA values support the observed degradation activity, it is important to note that these calculations alone cannot fully predict PROTAC efficacy. Other critical factors, such as cellular uptake, target engagement, and efficacy of the target ubiquitination also influencing overall proteasomal target degradation in cells.

*3.3.3.2. Calculation of the BSA and Rg.* To further assess the stability of the ATR ternary complexes, particularly at the protein-protein interface, the BSA and Rg were calculated (Fig. S29 and S30). The Rg values for all complexes remained consistent at approximately 39 Å, indicating a high degree of structural stability and compactness. In contrast, the BSA values varied across the different complexes. For PROTACs 42i, 12b and ZS-7, the BSA fluctuated between 2000 and 2500 $Å^2$, while for 8i and 10b, the BSA stabilized around 1500 $Å^2$. These variations are likely due to the dependency of BSA calculations on SASA measurements. Small structural changes, such as side chain conformations, can impact the SASA [74] of a structure, leading to different BSA values. Despite these variations, the BSA plots showed minimal deviations and remained stable for all ternary complexes. Altogether, the results further confirm the stability of the ATR ternary complexes and the integrity of the protein-protein interface. Additionally, the second replicate exhibited results closely aligned with the first, reinforcing the stability and reliability of the simulations.

In summary, the results derived from the MD simulations confirm

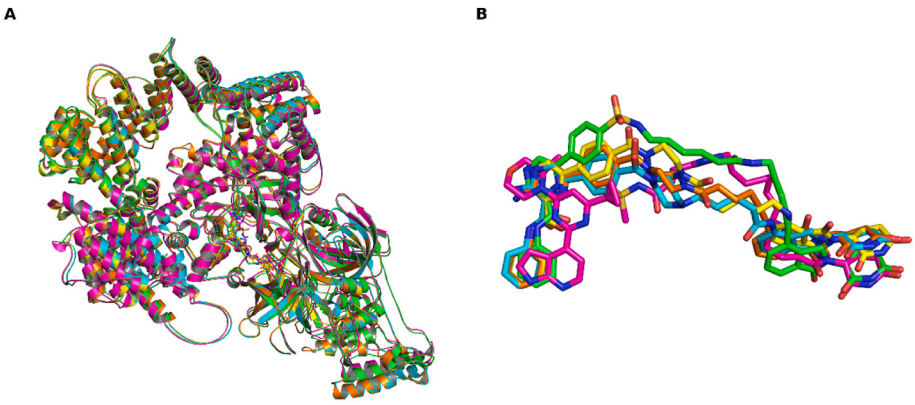


**Fig. 4.** Superposition of the generated ATR/CRBN ternary complexes. The complexes are colored as follows: 42i (Abd110) (green), 8i (cyan), 10b (yellow), 12b (orange) and ZS-7 (magenta). In (A), the complete ternary complexes are displayed after superposition of the Cα atoms of the protein backbones. (B) shows the PROTAC structures after the superposition of the Cα atoms of the binding sites. (For interpretation of the references to color in this figure legend, the reader is referred to the Web version of this article.)

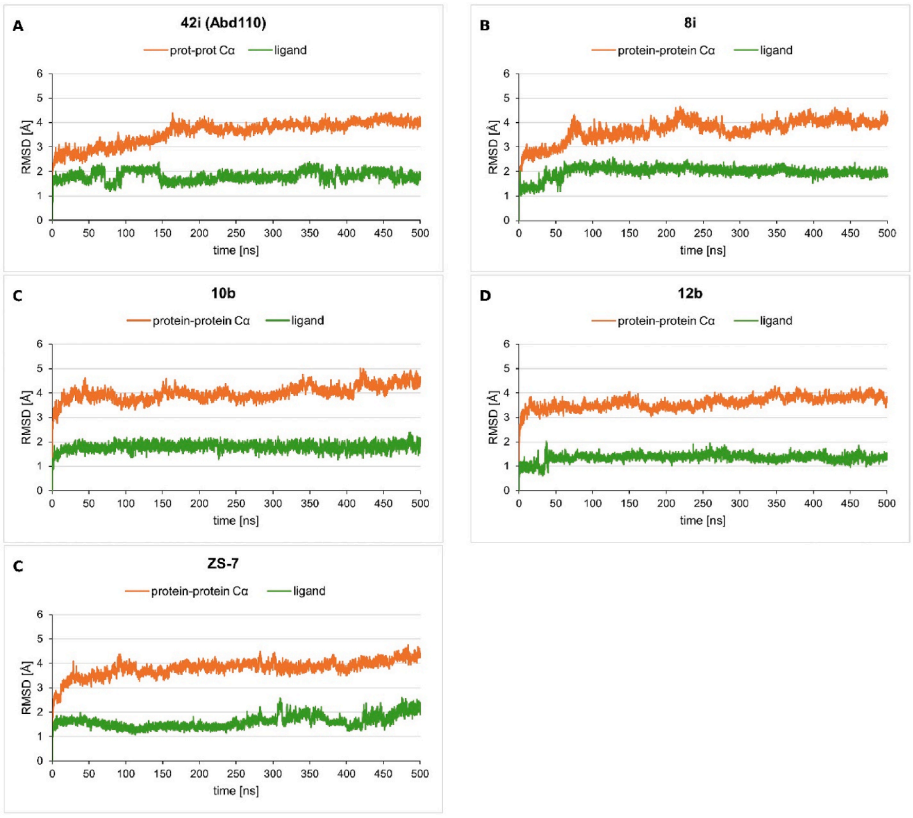


**Fig. 5.** Results for the first 500 ns MD simulations of the ATR ternary complexes. RMSD plots are displayed for the protein-protein Cα atoms of the protein backbone and the heavy atoms of the PROTACs. They are shown as follows: (A) 42i (Abd110), (B) 8i, (C) 10b, (D) 12b and (E) ZS-7.

that all five modeled ATR ternary complexes remained stable over the 500 ns simulation period. Despite the variations in the linker length, all PROTACs consistently adopt a very similar protein conformation for both partners and exhibited stability throughout the simulation. Minor derivation observed in the RMSD, Rg and BSA curves can be attributed to differences in linker length and small variations in the protein conformation during the simulation. While MD simulations provide valuable insights into the behavior of the reported ATR PROTACs, they cannot fully predict their efficacy. Critical features such as cellular uptake, permeability, and target ubiquitination are essential for evaluating the overall effectiveness of PROTACs in a biological context. Nevertheless, the simulations underscore the consistent binding of the warheads to the ATR kinase and CRBN. In addition, regions of higher flexibility and linker dynamics, as observed for ZS-7, were revealed. The degradation activity of the PROTACs was further supported by MMGBSA binding free energy calculations, which confirmed the binding stability of the PROTACs.

## 4. Conclusion

In this study, a novel computational approach for modeling ternary complexes was introduced. The combination of protein-protein docking using HADDOCK and induced fit docking proved its efficiency, as validated by 26 ternary complex structures. Particularly for CRBN-based

ternary complexes, such as PDB IDs 6BOY and 6BN7, highly accurate results were achieved. Furthermore, MD simulations were utilized to confirm the stability of the crystal structures PDB ID 6BOY and 6BN7. By incorporating two additional parameters, Rg and BSA, a more profound understanding of the compactness and stability of the protein-protein interface was obtained. Additionally, ternary complexes for five active ATR degraders were generated using the proposed methodology. The utilization of an optimized AlphaFold structure for the ATR kinase enabled the overcoming of the lack of suitable ATR crystal structures for complex modeling. Despite variations in warhead structures and linker lengths, a similar protein-protein conformation was obtained across all ternary complexes. This finding suggests that active ATR PROTACs can adopt the same protein-protein conformation, regardless of the linker length. The reliability of these models was further supported by MD simulations, which revealed only minor differences depending on the PROTAC structure. Overall, the results highlight the utility of this computational approach in the structural design of CRBN-based PROTACs. In light of these findings, it can be concluded that this method can be further applied to optimize existing structures and contribute to the development of novel ATR degraders. Furthermore, the method offers a valuable framework for modeling ternary complexes of diverse target proteins, providing insights into protein-protein conformations and facilitating the rational design of new PROTACs.

Nevertheless, several limitations of the employed methodologies have to be considered. For the protein-protein docking in HADDOCK, challenges arose in complexes with fewer or missing protein-protein interactions, as observed in WDR5-VHL ternary complexes (PDB IDs 8BB2 and 8BB3). These structures also pose challenges during MD simulations as they displayed unstable RMSD and BSA values. With regard to ternary complexes with limited protein-protein interactions, further validation and the exploration of novel approaches are imperative for future progress in PROTAC development.

## CRediT authorship contribution statement

**Anne-Christin Sarnow:** Writing – original draft, Visualization, Software, Methodology, Investigation, Formal analysis. **Husam Nassar:** Software, Methodology. **Abdallah M. Alfayomy:** Methodology, Investigation. **Dina Robaa:** Writing – review & editing. **Wolfgang Sippl:** Writing – review & editing, Supervision, Resources, Data curation, Conceptualization.

## Ethics in publishing statement

I testify on behalf of all co-authors that our article submitted followed ethical principles in publishing.

All authors agree that:

This research presents an accurate account of the work performed, all data presented are accurate and methodologies detailed enough to permit others to replicate the work.

This manuscript represents entirely original works and or if work and/or words of others have been used, that this has been appropriately cited or quoted and permission has been obtained where necessary.

This material has not been published in whole or in part elsewhere.

The manuscript is not currently being considered for publication in another journal.

That generative AI and AI-assisted technologies have not been utilized in the writing process or if used, disclosed in the manuscript the use of AI and AI-assisted technologies and a statement will appear in the published work.

That generative AI and AI-assisted technologies have not been used to create or alter images unless specifically used as part of the research design where such use must be described in a reproducible manner in the methods section.

All authors have been personally and actively involved in substantive work leading to the manuscript and will hold themselves jointly and individually responsible for its content.

Corresponding author's name: Prof. Dr. Wolfgang Sippl.

Date: March 05, 2025.

## Declaration of competing interest

The authors declare that they have no known competing financial interests or personal relationships that could have appeared to influence the work reported in this paper.

Prof. Wolfgang Sippl on behalf of all coauthors.

## Acknowledgement

This work was funded by the Deutsche Forschungsgemeinschaft (DFG) project number 528202295 (to W.S). A.-C.S. acknowledges funding by the Landesgraduiertenförderung Saxony-Anhalt.

## Appendix A. Supplementary data

Supplementary data to this article can be found online at https://doi.org/10.1016/j.compbiomed.2025.110570.

## References

[1] T.K. Neklesa, J.D. Winkler, C.M. Crews, Targeted protein degradation by PROTACs, Pharmacol. Ther. 174 (2017) 138–144, https://doi.org/10.1016/j.pharmthera.2017.02.027.

[2] M. Pettersson, C.M. Crews, PROteolysis TArgeting Chimeras (PROTACs) - past, present and future, Drug Discov. Today Technol. 31 (2019) 15–27, https://doi.org/10.1016/j.ddtec.2019.01.002.

[3] M. Toure, C.M. Crews, Small-molecule PROTACS: new approaches to protein degradation, Angew Chem. Int. Ed. Engl. 55 (6) (2016) 1966–1973, https://doi.org/10.1002/anie.201507978.

[4] D.L. Buckley, C.M. Crews, Small-molecule control of intracellular protein levels through modulation of the ubiquitin proteasome system, Angew Chem. Int. Ed. Engl. 53 (9) (2014) 2312–2330, https://doi.org/10.1002/anie.201307761.

[5] E. Bulatov, A. Ciulli, Targeting Cullin-RING E3 ubiquitin ligases for drug discovery: structure, assembly and small-molecule modulation, Biochem. J. 467 (3) (2015) 365–386, https://doi.org/10.1042/bj20141450.

[6] R. Verma, D. Mohl, R.J. Deshaies, Harnessing the power of proteolysis for targeted protein inactivation, Mol Cell 77 (3) (2020) 446–460, https://doi.org/10.1016/j.molcel.2020.01.010.

[7] G.E. Winter, et al., DRUG DEVELOPMENT. Phthalimide conjugation as a strategy for in vivo target protein degradation, Science 348 (6241) (2015) 1376–1381, https://doi.org/10.1126/science.aab1433.

[8] M. Zengerle, K.H. Chan, A. Ciulli, Selective small molecule induced degradation of the BET bromodomain protein BRD4, ACS Chem. Biol. 10 (8) (2015) 1770–1777, https://doi.org/10.1021/acschembio.5b00216.

[9] Y. Itoh, et al., Protein knockdown using methyl Bestatin−Ligand hybrid molecules: design and synthesis of inducers of ubiquitination-mediated degradation of cellular retinoic acid-binding proteins, J. Am. Chem. Soc. 132 (16) (2010) 5820–5826, https://doi.org/10.1021/ja100691p.

[10] C. Wang, et al., Developments of CRBN-based PROTACs as potential therapeutic agents, Eur. J. Med. Chem. 225 (2021) 113749, https://doi.org/10.1016/j.ejmech.2021.113749.

[11] G. Apprato, et al., Exploring the chemical space of orally bioavailable PROTACs, Drug Discov. Today 29 (4) (2024) 103917, https://doi.org/10.1016/j.drudis.2024.103917.

[12] W. Huang, et al., Progress on small-molecule proteolysis-targeting chimeras, Future Med. Chem. 11 (20) (2019) 2715–2734, https://doi.org/10.4155/fmc-2019-0161.

[13] Y. Liang, K.S. Nandakumar, K. Cheng, Design and pharmaceutical applications of proteolysis-targeting chimeric molecules, Biochem. Pharmacol. 182 (2020) 114211, https://doi.org/10.1016/j.bcp.2020.114211.

[14] X. Sun, et al., PROTACs: great opportunities for academia and industry, Signal Transduct Target Ther 4 (2019) 64, https://doi.org/10.1038/s41392-019-0101-6.

[15] X. Zhou, et al., PROTAC: a promising technology for cancer treatment, Eur. J. Med. Chem. 203 (2020) 112539, https://doi.org/10.1016/j.ejmech.2020.112539.

[16] D.P. Bondeson, et al., Catalytic in vivo protein knockdown by small-molecule PROTACs, Nat. Chem. Biol. 11 (8) (2015) 611–617, https://doi.org/10.1038/nchembio.1858.

[17] D.P. Bondeson, et al., Lessons in PROTAC design from selective degradation with a promiscuous warhead, Cell Chem. Biol. 25 (1) (2018) 78–87 e5, https://doi.org/10.1016/j.chembiol.2017.09.010.

[18] A.C. Lai, C.M. Crews, Induced protein degradation: an emerging drug discovery paradigm, Nat. Rev. Drug Discov. 16 (2) (2017) 101–114, https://doi.org/10.1038/nrd.2016.211.

[19] S.D. Edmondson, B. Yang, C. Fallan, Proteolysis targeting chimeras (PROTACs) in 'beyond rule-of-five' chemical space: recent progress and future challenges, Bioorg.

Med. Chem. Lett 29 (13) (2019) 1555–1564, https://doi.org/10.1016/j.bmcl.2019.04.030.
[20] H.J. Maple, et al., Developing degraders: principles and perspectives on design and chemical space, MedChemComm 10 (10) (2019) 1755–1764, https://doi.org/10.1039/C9MD00272C.
[21] K.H. Chan, et al., Impact of target warhead and linkage vector on inducing protein degradation: comparison of bromodomain and extra-terminal (BET) degraders derived from triazolodiazepine (JQ1) and tetrahydroquinoline (I-BET726) BET inhibitor scaffolds, J. Med. Chem. 61 (2) (2018) 504–513, https://doi.org/10.1021/acs.jmedchem.6b01912.
[22] K. Cyrus, et al., Jostling for position: optimizing linker location in the design of estrogen receptor-targeting PROTACs, ChemMedChem 5 (7) (2010) 979–985, https://doi.org/10.1002/cmdc.201000146.
[23] S. Shaik, et al., Advances in designing ternary complexes: integrating in-silico and biochemical methods for PROTAC optimisation in target protein degradation, Bioorg. Chem. 153 (2024) 107868, https://doi.org/10.1016/j.bioorg.2024.107868.
[24] M.L. Drummond, et al., Improved accuracy for modeling PROTAC-mediated ternary complex formation and targeted protein degradation via new in silico methodologies, J. Chem. Inf. Model. 60 (10) (2020) 5234–5254, https://doi.org/10.1021/acs.jcim.0c00897.
[25] M.L. Drummond, C.I. Williams, In silico modeling of PROTAC-mediated ternary complexes: validation and application, J. Chem. Inf. Model. 59 (4) (2019) 1634–1644, https://doi.org/10.1021/acs.jcim.8b00872.
[26] G. Weng, et al., Integrative modeling of PROTAC-mediated ternary complexes, J. Med. Chem. 64 (21) (2021) 16271–16281, https://doi.org/10.1021/acs.jmedchem.1c01576.
[27] D. Zaidman, J. Prilusky, N. London, PRosettaC: rosetta based modeling of PROTAC mediated ternary complexes, J. Chem. Inf. Model. 60 (10) (2020) 4894–4903, https://doi.org/10.1021/acs.jcim.0c00589.
[28] H. Kumar, M.E. Sobhia, Interplay of PROTAC complex dynamics for undruggable targets: insights into ternary complex behavior and linker design, ACS Med. Chem. Lett. 15 (8) (2024) 1306–1318, https://doi.org/10.1021/acsmedchemlett.4c00189.
[29] R.P. Wurz, et al., Affinity and cooperativity modulate ternary complex formation to drive targeted protein degradation, Nat. Commun. 14 (1) (2023) 4177, https://doi.org/10.1038/s41467-023-39904-5.
[30] R.P. Law, et al., Discovery and characterisation of highly cooperative FAK-degrading PROTACs, Angew Chem. Int. Ed. Engl. 60 (43) (2021) 23327–23334, https://doi.org/10.1002/anie.202109237.
[31] S. Imaide, et al., Trivalent PROTACs enhance protein degradation via combined avidity and cooperativity, Nat. Chem. Biol. 17 (11) (2021) 1157–1167, https://doi.org/10.1038/s41589-021-00878-4.
[32] T.H. Pillow, et al., Antibody conjugation of a chimeric BET degrader enables in vivo activity, ChemMedChem 15 (1) (2020) 17–25, https://doi.org/10.1002/cmdc.201900497.
[33] C. Maniaci, et al., Homo-PROTACs: bivalent small-molecule dimerizers of the VHL E3 ubiquitin ligase to induce self-degradation, Nat. Commun. 8 (1) (2017) 830, https://doi.org/10.1038/s41467-017-00954-1.
[34] J. Schiemer, et al., Snapshots and ensembles of BTK and cIAP1 protein degrader ternary complexes, Nat. Chem. Biol. 17 (2) (2021) 152–160, https://doi.org/10.1038/s41589-020-00686-2.
[35] R.I. Troup, C. Fallan, M.G.J. Baud, Current strategies for the design of PROTAC linkers: a critical review, Explor Target Antitumor Ther. 1 (5) (2020) 273–312, https://doi.org/10.37349/etat.2020.00018.
[36] R.V. Honorato, et al., Structural biology in the clouds: the WeNMR-EOSC ecosystem, Front. Mol. Biosci. 8 (2021).
[37] R.V. Honorato, et al., The HADDOCK2.4 web server for integrative modeling of biomolecular complexes, Nat. Protoc. 19 (11) (2024) 3219–3241, https://doi.org/10.1038/s41596-024-01011-0.
[38] C.C.G. Inc, Molecular Operating Environment (MOE) Version 2019.0102, Chemical Computing Group Inc, Montreal, 2019.
[39] J.C. Saldivar, D. Cortez, K.A. Cimprich, The essential kinase ATR: ensuring faithful duplication of a challenging genome, Nat. Rev. Mol. Cell Biol. 18 (10) (2017) 622–636, https://doi.org/10.1038/nrm.2017.67.
[40] A.M. Alfayomy, et al., Design, synthesis, and biological characterization of proteolysis targeting chimera (PROTACs) for the ataxia telangiectasia and RAD3-related (ATR) kinase, Eur. J. Med. Chem. 267 (2024) 116167, https://doi.org/10.1016/j.ejmech.2024.116167.
[41] Y. Wang, et al., Discovery of selective and potent ATR degrader for exploration its kinase-independent functions in acute myeloid leukemia cells, Angew Chem. Int. Ed. Engl. 63 (17) (2024) e202318568, https://doi.org/10.1002/anie.202318568.
[42] L. Huang, et al., Discovery of the first ataxia telangiectasia and Rad3-related (ATR) degraders for cancer treatment, Eur. J. Med. Chem. 267 (2024) 116159, https://doi.org/10.1016/j.ejmech.2024.116159.
[43] S. Release, Schrödinger, LLC, New York, NY, 2021.
[44] P.P. Wizard, et al., LLC, 2021, p. 34. New York, NY.
[45] G.M. Sastry, et al., Ligand preparation: parameters, protocols, and influence on virtual screening enrichments, J. Comput. Aided Mol. Des. 27 (2013) 221–234, https://doi.org/10.1007/s10822-013-9644-8.
[46] W.L. Jorgensen, D.S. Maxwell, J. Tirado-Rives, Development and testing of the OPLS all-atom force field on conformational energetics and properties of organic liquids, J. Am. Chem. Soc. 118 (45) (1996) 11225–11236, https://doi.org/10.1021/ja9621760.
[47] W.L. Jorgensen, J. Tirado-Rives, The OPLS [optimized potentials for liquid simulations] potential functions for proteins, energy minimizations for crystals of cyclic peptides and crambin, J. Am. Chem. Soc. 110 (6) (1988) 1657–1666, https://doi.org/10.1021/ja00214a001.
[48] D. Shivakumar, et al., Prediction of absolute solvation free energies using molecular dynamics free energy perturbation and the OPLS force field, J. Chem. Theor. Comput. 6 (5) (2010) 1509–1519, https://doi.org/10.1021/ct900587b.
[49] C. Lu, et al., OPLS4: improving force field accuracy on challenging regimes of chemical space, J. Chem. Theor. Comput. 17 (7) (2021) 4291–4300, https://doi.org/10.1021/acs.jctc.1c00302.
[50] S. Release, LigPrep, Schrödinger, LLC, New York, NY, 2021.
[51] R.C. Johnston, et al., Epik: pKa and protonation state prediction through machine learning, J. Chem. Theor. Comput. 19 (8) (2023) 2380–2388, https://doi.org/10.1021/acs.jctc.3c00044.
[52] S. ConfGen, LLC, 2021. New York, NY.
[53] Y. Lu, et al., Rationally designed PI3Kα mutants to mimic ATR and their use to understand binding specificity of ATR inhibitors, J. Mol. Biol. 429 (11) (2017) 1684–1704, https://doi.org/10.1016/j.jmb.2017.04.006.
[54] S. Release, Glide, Schrödinger, LLC vol. 3, Schrödinger Release, New York, NY, 2021, p. 2021.
[55] R.A. Friesner, et al., Glide: a new approach for rapid, accurate docking and scoring. 1. Method and assessment of docking accuracy, J. Med. Chem. 47 (7) (2004) 1739–1749, https://doi.org/10.1021/jm0306430.
[56] T.A. Halgren, et al., Glide: a new approach for rapid, accurate docking and scoring. 2. Enrichment factors in database screening, J. Med. Chem. 47 (7) (2004) 1750–1759, https://doi.org/10.1021/jm030644s.
[57] R.A. Friesner, et al., Extra precision Glide: docking and scoring incorporating a model of hydrophobic enclosure for Protein−Ligand complexes, J. Med. Chem. 49 (21) (2006) 6177–6196, https://doi.org/10.1021/jm051256o.
[58] Y. Yang, et al., Efficient exploration of chemical space with docking and deep learning, J. Chem. Theor. Comput. 17 (11) (2021) 7106–7119, https://doi.org/10.1021/acs.jctc.1c00810.
[59] C. Dominguez, R. Boelens, A.M.J.J. Bonvin, HADDOCK: a Protein−Protein docking approach based on biochemical or biophysical information, J. Am. Chem. Soc. 125 (7) (2003) 1731–1737, https://doi.org/10.1021/ja026939x.
[60] S. Release, Desmond Molecular Dynamics System, DE Shaw Research, Maestro-Desmond Interoperability Tools, New York, NY, 2021. Schrödinger, New York, NY, 2021. 2021.
[61] Proceedings of the 2006 ACM/IEEE Conference on Supercomputing, Association for Computing Machinery, Tampa, Florida, 2006.
[62] G.J. Martyna, M.L. Klein, M. Tuckerman, Nosé–Hoover chains: the canonical ensemble via continuous dynamics, The Journal of chemical physics 97 (4) (1992) 2635–2643.
[63] G.J. Martyna, D.J. Tobias, M.L. Klein, Constant pressure molecular dynamics algorithms, The Journal of chemical physics 101 (5) (1994) 4177–4189.
[64] J. Li, et al., The VSGB 2.0 model: a next generation energy model for high resolution protein structure modeling, Proteins 79 (10) (2011) 2794–2812, https://doi.org/10.1002/prot.23106.
[65] P. Narang, et al., A computational pathway for bracketing native-like structures for small alpha helical globular proteins, Phys. Chem. Chem. Phys. 7 (11) (2005) 2364–2375, https://doi.org/10.1039/B502226F.
[66] H. William, D. Andrew, S. Klaus, VMD – V isual M olecular D ynamics, J. Mol. Graph. 14 (1996) 33–38.
[67] E. Rovers, M. Schapira, Benchmarking methods for PROTAC ternary complex structure prediction, J. Chem. Inf. Model. 64 (15) (2024) 6162–6173, https://doi.org/10.1021/acs.jcim.4c00426.
[68] R.P. Nowak, et al., Plasticity in binding confers selectivity in ligand-induced protein degradation, Nat. Chem. Biol. 14 (7) (2018) 706–714, https://doi.org/10.1038/s41589-018-0055-y.
[69] H. Zhao, Structural Basis of conformational dynamics in the PROTAC-induced protein degradation, ChemMedChem 19 (14) (2024) e202400171, https://doi.org/10.1002/cmdc.202400171.
[70] Q. Rao, et al., Cryo-EM structure of human ATR-ATRIP complex, Cell Res. 28 (2) (2018) 143–156, https://doi.org/10.1038/cr.2017.158.
[71] A.G. Kansy, et al., Pharmacological degradation of ATR induces antiproliferative DNA replication stress in leukemic cells, Mol. Oncol. 18 (8) (2024) 1958–1965, https://doi.org/10.1002/1878-0261.13638.
[72] S. Genheden, U. Ryde, The MM/PBSA and MM/GBSA methods to estimate ligand-binding affinities, Expert Opin Drug Discov 10 (5) (2015) 449–461, https://doi.org/10.1517/17460441.2015.1032936.
[73] W. Li, et al., Importance of three-body problems and protein–protein interactions in proteolysis-targeting chimera modeling: insights from molecular dynamics simulations, J. Chem. Inf. Model. 62 (3) (2022) 523–532, https://doi.org/10.1021/acs.jcim.1c01150.
[74] J.A. Marsh, S.A. Teichmann, Relative solvent accessible surface area predicts protein conformational changes upon binding, Structure 19 (6) (2011) 859–867, https://doi.org/10.1016/j.str.2011.03.010.